Check for updates

JGR Oceans

RESEARCH ARTICLE
10.1029/2026JC024509

Away From Glacier Termini, Turbulent Mixing Plays a Minor Role in Early-Summer Nutrient Supply in a Northwest Greenland Fjord

K. Schulz[1], L. Meire[2,3], I. Fer[4], D. Fahrner[5], K. Zhao[6], S. Maier[2], L. Ponsoni[7], and W. Boone[7]

[1]Oden Institute for Computational Engineering and Sciences, The University of Texas at Austin, Austin, TX, USA, [2]Greenland Climate Research Centre, Greenland Institute of Natural Resources, Nuuk, Greenland, [3]Department of Estuarine and Delta Systems, Royal Netherlands Institute of Sea Research (NIOZ), Utrecht University, Yerseke, The Netherlands, [4]Geophysical Institute, University of Bergen and Bjerknes Centre for Climate Research, Bergen, Norway, [5]Department of Glaciology and Climate, Geological Survey of Denmark and Greenland, Copenhagen, Denmark, [6]University of North Carolina at Chapel Hill, Chapel Hill, NC, USA, [7]Marine Robotics Centre, Flanders Marine Institute, Ostend, Belgium

Key Points:

- Turbulent dissipation rates and turbulent vertical nutrient fluxes during early summer are consistently low in the fjords around Uummannaq
- Enhanced dissipation and nutrient fluxes near a detached plume 3 km from the glacier reveal an additional vertical transport mechanism
- Fjord-wide turbulent nutrient transport is an order of magnitude smaller than the estimated transport from one subglacial discharge plume

Supporting Information:

Supporting Information may be found in the online version of this article.

Correspondence to:

K. Schulz,
kiki.schulz@utexas.edu

Citation:

Schulz, K., Meire, L., Fer, I., Fahrner, D., Zhao, K., Maier, S., et al. (2026). Away from glacier termini, turbulent mixing plays a minor role in early-summer nutrient supply in a northwest Greenland fjord. *Journal of Geophysical Research: Oceans*, *131*, e2026JC024509. https://doi.org/10.1029/2026JC024509

Received 24 APR 2026
Accepted 4 NOV 2026

Author Contributions:

Conceptualization: K. Schulz, L. Meire, W. Boone
Data curation: K. Schulz, L. Meire, L. Ponsoni
Formal analysis: K. Schulz, L. Meire, D. Fahrner
Funding acquisition: L. Meire, W. Boone
Investigation: K. Schulz

© 2026 The Author(s). Journal of Geophysical Research: Oceans published by Wiley Periodicals LLC on behalf of American Geophysical Union.
This is an open access article under the terms of the Creative Commons Attribution-NonCommercial License, which permits use, distribution and reproduction in any medium, provided the original work is properly cited and is not used for commercial purposes. All other rights reserved, including rights for text and data mining and training of artificial intelligence technologies or similar technologies.

Abstract

Marine-terminating glaciers strongly influence nutrient supply and ecosystem productivity in Greenland fjords. However, the relative contributions of subglacial discharge plumes, vertical turbulent mixing and other processes to the surface nutrient supply remain poorly constrained. Here, we present co-located observations of turbulence, nutrient distributions, and primary production collected in the fjord system around Uummannaq in northwest Greenland in the beginning of July 2022, covering the region 3 km from the terminus and outward into the fjord system. Turbulent dissipation rates and associated vertical nitrate fluxes were generally low throughout the fjord, with fluxes of around 0.1 mmol m^{-2} d^{-1}, consistent with strongly stratified and rather quiescent Arctic environments. In contrast, elevated turbulence and nutrient fluxes were observed in the vicinity of a detached subglacial discharge plume, revealing a secondary mechanism for localized vertical transport linked to plume dynamics, in addition to entrainment of deep water during plume ascent. Despite this enhancement, fjord-integrated turbulent nutrient supply was an order of magnitude smaller than estimates of nutrient transport associated with entrainment and upward transport in a single subglacial discharge plume at the glacier terminus. Primary production was high across the fjord and largely decoupled from spatial variability in turbulent nutrient fluxes, suggesting that localized nutrient supply is not controlling productivity at this time. These results demonstrate that subglacial plumes can dominate vertical nutrient supply in glaciated fjords, while turbulent mixing plays a comparatively minor role, implying major consequences for the ecosystem response to marine-terminating glacier retreat.

Plain Language Summary

Glacial fjords in West Greenland are hotspots of marine life. One key reason is that where glaciers end in the ocean, meltwater from the ice sheet is released at depth. This fresh water forms plumes that rise to the surface and bring nutrient-rich deep water with them, stimulating phytoplankton growth. However, plumes are not the only way nutrients can reach the surface. Other processes like turbulent mixing in the water column also play a role, but the exact contribution of any of these processes is still not well understood. As the climate warms and glaciers retreat onto land, we need to quantify all nutrients transport mechanisms to better predict how fjord ecosystems may change. In this study, we measured nutrient transported in a Greenland fjord by vertical mixing, covering the fjord system up to 3 km from the glacier front. We found that mixing and nutrient transport were low, except downstream of a subglacial discharge plume, and ascending plumes are far more efficient in bringing nutrients to the surface. Primary productivity was high throughout the fjord. Our data sets and findings help clarify bloom dynamics, how fjord ecosystems function today and how they may respond to glacier retreat.

1. Introduction

Greenland's glaciated fjords and coastal regions host productive ecosystems (Meire et al., 2017), essential to Greenlandic livelihoods and Greenland's economy, including fishery export. The functioning of these marine ecosystems depends on whether or not local conditions favor large phytoplankton blooms, which are the basis of the food web, sustaining zooplankton, fish, mammals and benthic ecosystems (Meire et al., 2017; Stuart-Lee

Methodology: K. Schulz, L. Meire, I. Fer, K. Zhao
Project administration: L. Meire, W. Boone
Software: K. Schulz
Validation: K. Schulz, L. Meire, I. Fer
Visualization: K. Schulz
Writing – original draft: K. Schulz, L. Meire, I. Fer, D. Fahrner, K. Zhao, S. Maier, L. Ponsoni, W. Boone
Writing – review & editing: K. Schulz, L. Meire, I. Fer, D. Fahrner, K. Zhao, S. Maier, L. Ponsoni, W. Boone

et al., 2023). The magnitude of phytoplankton blooms or primary productivity is regulated by the nutrient availability in the photic zone, which is limited by the upward transport from deep, nutrient-rich water layers (e.g., Schulz et al., 2022; Waite et al., 2026).

Marine-terminating glaciers are recognized as an important factor for a productive fjord ecosystem during summer. Meltwater from the ice sheet is discharged at the grounding line of glaciers and entrains deep waters when rising to the surface, providing a transport pathway for deep nutrients to the photic zone (Cape et al., 2019; Hopwood et al., 2020; Kanna et al., 2018, 2020, 2022; Meire et al., 2017). Surface run-off of turbid glacial meltwater, on the other hand, can limit nutrient and light availability, with adverse effects on primary production, leaving these fjords much less productive (e.g., Young Sound in East Greenland, Holding et al., 2019). As an example, Nuup Kangerlua, a fjord fed by marine-terminating glaciers, sustains high phytoplankton productivity that is dominated by diatoms and grazed by larger mesozooplankton throughout summer, while the ecosystem in the adjacent Ameralik, fed only by land-terminating glaciers, is dominated by bacteria, picophytoplankton and smaller zooplankton (Stuart-Lee et al., 2023). The annual primary productivity in Ameralik is only one-third of the productivity compared to Nuup Kangerlua (Meire et al., 2023).

With global warming, many marine-terminating glaciers are retreating (Catania et al., 2018; Greene, Gardner, et al., 2024) to shallower waters and ultimately on land, and their associated nutrient supply mechanisms will disappear (Hopwood et al., 2018). Already between 2000 and 2020, 7.2% of the glaciers in the Northern Hemisphere ceased to be marine-terminating (Kochtitzky & Copland, 2022), underscoring the rapid pace of this transition. A quantitative understanding of nutrient supply mechanisms tied to marine-terminating glaciers, and supply mechanisms that will persist in the future will help local subsistence and commercial harvesters prepare for ecosystem changes in fjords and surrounding coastal waters.

Despite their importance, nutrient budgets in glacial fjords remain poorly constrained due to limited observations. To date, co-located turbulence and nutrient observations in coastal Greenland exist only from Young Sound (Randelhoff et al., 2020), a Northeast Greenland fjord influenced by land-terminating rather than marine-terminating glaciers.

The specific seasonal bloom dynamics in the fjord system around Uummannaq have not been investigated in detail. Generally, the onset of pelagic productivity in the Arctic is determined by increasing light availability when sea ice retreats (e.g., Ardyna & Arrigo, 2020). Nutrients delivered to the surface by rising subglacial discharge plumes maintain high levels of productivity throughout the melting season in glaciated fjords (Kanna et al., 2022; Meire et al., 2017; Stuart-Lee et al., 2023). Depending on the upper ocean stratification and exact pathways of nutrient supply, blooms are often located subsurface later in the productive season, when surface nutrients are depleted (Lee et al., 2012; Rudels et al., 1991).

Here, we present a survey of turbulent mixing, nutrient distributions, and primary production in a West Greenland fjord (Figure 1), enabling direct quantification of vertical nutrient fluxes in a glacial environment. Our objective is to quantify turbulent mixing and vertical nitrate fluxes and to assess their role in supporting primary production across the fjord system. Details on sampling and data processing are given in Section 2, followed by a description of the study site, environmental conditions, and fjord hydrography in Section 3. Results on turbulent mixing, nitrate fluxes, and primary production are presented in Section 4, followed by a discussion of nutrient supply mechanisms in Section 5, and conclusions in Section 6.

2. Methods

Data were collected aboard R/V Sanna in the fjord system near Uummannaq, West Greenland, between 28 June and 10 July 2022 (Figure 2a). Sampling included ship-based profiles of a CTD (conductivity, temperature, depth) system (Sea-Bird Scientific SBE19plus) with an attached optical nitrate sensor (SUNA v2 - Submersible Ultraviolet Nitrate Analyzer, Sea-Bird Scientific; gray dots in Figure 2a). At selected stations, we obtained discrete nutrient samples and vertical microstructure profiles (VMP250-IR, Rockland Scientific Inc., VMP hereafter, black crosses in Figure 2a) concurrent with or shortly after CTD casts, and water samples for incubation to quantify primary production.

The VMP was ballasted for sinking profiling mode and equipped with two air-foil shear probes, two fast-response FP07 thermistors, a CTD sensor, and an optical sensor for chlorophyll-a fluorescence and turbidity. All sensors

21699291, 2026, 11, Downloaded from https://agupubs.onlinelibrary.wiley.com/doi/10.1029/2026JC024509, Wiley Online Library on [16/11/2026]. See the Terms and Conditions (https://onlinelibrary.wiley.com/terms-and-conditions) on Wiley Online Library for rules of use; OA articles are governed by the applicable Creative Commons License

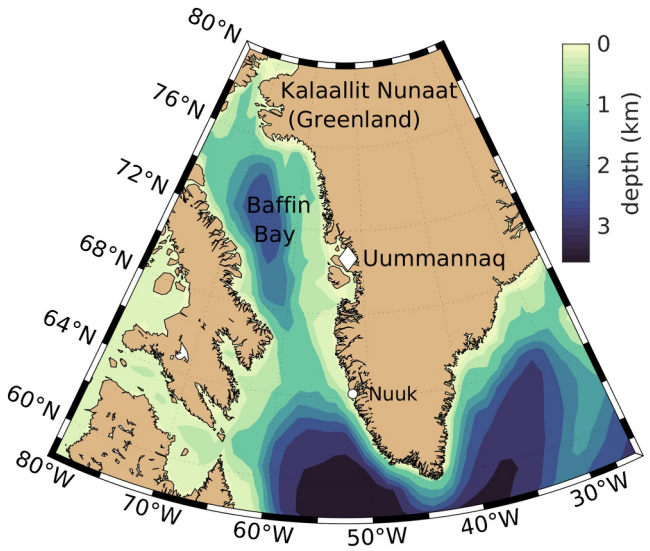


Figure 1. Bathymetric map of the region around Greenland, with the location of the study region near Uummannaq indicated (white diamond).

were factory-calibrated before the cruise. The profiler was deployed from a workboat about 100 m from R/V Sanna, or directly from the ship. At each station, at least four successive profiles were collected, and GPS coordinates were logged at the start of each profile. For three profiles without GPS data, positions were interpolated. Shear probe data were processed following Lueck et al. (2024), with all parameter choices and metadata included in the published data set (Schulz, 2025). Temperature and salinity were converted to Conservative Temperature (°C) and Absolute Salinity (g kg^{-1}) using the TEOS-10 equation of state (McDougall & Barker, 2011). Turbidity data were calibrated against co-located SBE19plus casts via least-squares fit and scaled by a factor of 2.0375 for consistency.

Water samples from discrete depths (1, 5, 10, 20, 30, 40, 50, and 100 m) were collected with a 5 L Niskin bottle. Subsamples (10 mL) were filtered through 0.45 µm filters (Q-Max GPF) and frozen at −20°C until analysis. Nutrients were measured by standard colorimetric methods on a Seal QuAAtro auto-analyzer. Detection limits are 0.10 µM for silicate, 0.05 µM for nitrate + nitrite and phosphate. The SUNA nitrate concentrations were calculated from the raw spectra (1 Hz) after subtracting the seawater (bromide) absorbance, corrected for in situ temperature, salinity and pressure (Plant et al., 2023; Sakamoto et al., 2009, 2017; Zheng et al., 2024) using CTD data. After quality control, data were averaged in 1 dbar bins and calibrated against the discrete samples (nitrate + nitrite, $n = 177$ from 20 stations) using a cruise-wide linear regression and an offset per cast (Meire, 2026 in Supporting Information S1).

The nitracline spans the depth range from the onset of increasing nitrate above surface-depleted levels to where concentrations stabilize at depth. Here, the upper bound of the nitracline is defined where nitrate exceeded 1 mmol m^{-3}, the lower bound where nitrate exceeds 80% of the mean concentration between 80 and 100 m. The gradient $\frac{\partial N}{\partial \sigma_\theta}$ is estimated from a linear regression of N against density across this range, the estimate is hence invariant to constant offsets in the nitrate data and robust to outliers and small-scale variability, including instrument noise. Nitrate and dissipation rate profiles were obtained with different instruments and consequently some spatio-temporal offset, and the density range rather than the depth range of the nitracline was used to select the respective vertical ε interval, to account for isopycnal displacement. Mean ε values were obtained using the maximum likelihood estimator (MLE, Baker & Gibson, 1987).

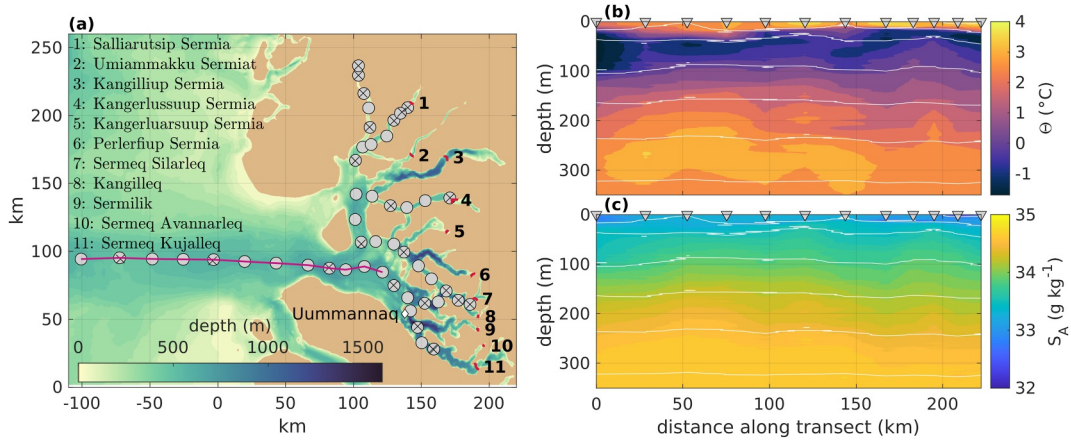


Figure 2. (a) Bathymetric map of the study region, with CTD sampling positions indicated in circles, turbulence sampling positions indicated with crosses, glacier termini (names according to Goliber et al., 2022) indicated in red, and the transect displayed in (b) and (c) indicated in magenta. West to east transect of (b) Conservative Temperature (°C) and (c) Absolute Salinity (g kg^{-1}), white lines in (b) and (c) indicate isopycnals with a spacing of 0.5 kg m^{-3}.

21699291, 2026, 11, Downloaded from https://agupubs.onlinelibrary.wiley.com/doi/10.1029/2026JC024509, Wiley Online Library on [16/11/2026]. See the Terms and Conditions (https://onlinelibrary.wiley.com/terms-and-conditions) on Wiley Online Library for rules of use; OA articles are governed by the applicable Creative Commons License

21699291, 2026, 11, Downloaded from https://agupubs.onlinelibrary.wiley.com/doi/10.1029/2026JC024509, Wiley Online Library on [16/11/2026]. See the Terms and Conditions (https://onlinelibrary.wiley.com/terms-and-conditions) on Wiley Online Library for rules of use; OA articles are governed by the applicable Creative Commons License

We calculate nutrient fluxes across the nitracline as

$$F_{\mathcal{N}} = K_z N^2 \frac{\rho}{g} \frac{\partial \mathcal{N}}{\partial \sigma_\theta}, \tag{1}$$

where $\mathcal{N}$ is the nitrate concentration in mmol m^{-3}, N^2 is the average buoyancy frequency squared in s^{-2}, K_z is the average vertical diffusivity in $m^2\ s^{-1}$ in the nitracline, $\rho = 1027$ kg m^{-3} is the seawater density and $g = 9.81$ m s^{-2} (Randelhoff et al., 2016; Schulz et al., 2022). Following literature standards, $F_{\mathcal{N}}$ is reported in mmol $m^{-2}\ d^{-1}$ (positive upward, Schulz et al., 2022). Vertical diffusivity K_z is calculated using the widely accepted parameterization provided in Bouffard and Boegman (2013) based on four mixing regimes, characterized by the buoyancy Reynolds number

$$Re_b = \frac{\varepsilon}{\nu N^2}. \tag{2}$$

In the molecular regime, $Re_b < 1.7$, that is, in quiescent conditions, molecular diffusion dominates and K_z equals to the molecular diffusivity K_m. At slightly higher $Re_b \leq 8.5$, strong stratification suppresses turbulent mixing and K_z scales with $Re_b^{1.5}$ (buoyancy controlled regime). In the transitional regime $8.5 < Re_b \leq 400$, K_z was found to linearly depend on Re_b, corresponding to a previous parameterization following Osborn (1980), using a constant mixing coefficient of $\Gamma = 0.2$. In the energetic regime $Re_b \geq 400$, $\Gamma = 0.2$ is an overestimate, and a better agreement was found for $K_z \sim Re_b^{0.5}$:

$$K_z = \begin{cases} K_m, & Re_b \leq 1.7 \\ 0.0615 \nu Re_b^{1.5}, & 1.7 < Re_b \leq 8.5 \\ \Gamma \nu Re_b, & 8.5 < Re_b \leq 400 \\ 4 \nu Re_b^{0.5}, & Re_b \geq 400. \end{cases} \tag{3}$$

Primary production rates are estimated using ^{14}C photosynthesis-irradiance (P-I) curve incubation. Samples from the surface (1 m) and chlorophyll maximum were incubated at in situ temperatures in a linear incubator with 12 light levels (0–800 µmol $m^{-2}\ s^{-1}$). The depth of the chlorophyll maximum was determined from fluorescence profiles and varied between stations (7–40 m). Samples were spiked with ^{14}C-bicarbonate and incubated for 2 hr following the protocol in Meire et al. (2015). Following incubation, samples were filtered onto 25 mm GF/F filters (Whatman), treated with 100 µL of 1 M HCl to remove excess inorganic ^{14}C. Filters were left open in a fume hood for 24 hr. Subsequently, 10 mL of scintillation cocktail (Ultima Gold, PerkinElmer) was added before counting on a liquid scintillation analyzer (Tri-Carb 2800 TR, PerkinElmer).

Gross primary production rates are calculated from the uptake of ^{14}C into particulate organic matter, correcting for dark fixation. No in situ solar irradiance data is available from local weather stations or the vessel. Therefore, incoming photosynthetically active radiation (PAR) is simulated using the *phytotools* package in *R* based on date, latitude, and longitude. We acknowledge that this theoretical approach does not account for cloud cover or topographic shading from the surrounding fjord walls, which likely leads to an overestimation of daily integrated production. However, this consistent approach minimizes inter-station bias, allowing for a comparison of relative primary production trends across the transect.

In addition to the data collected during the expedition, a number of existing data sets are used to provide background information. Bathymetric data was taken from IceBridge BedMachine Greenland, Version 5 (Morlighem et al., 2022). Meteorological data were obtained from the Mittarfik Uummannaq–Qaarsut weather station (Danish Meteorological Institute ID 04213). Sentinel-2 images illustrating sea ice conditions were provided by the European Space Agency (Copernicus program). Glacier terminus positions were manually delineated from Landsat-8/9 and Sentinel-2 imagery using the Google Earth Engine Digitization Tool (Lea, 2018), with errors smaller than Landsat pixel size (Fahrner et al., 2021). Terminus changes were quantified using the curvilinear box method in the Margin Change Quantification Tool (Lea, 2018). Runoff was taken from a daily discharge product (Mankoff, 2020; Mankoff et al., 2020), which relies on 7.5 km resolution Modèle

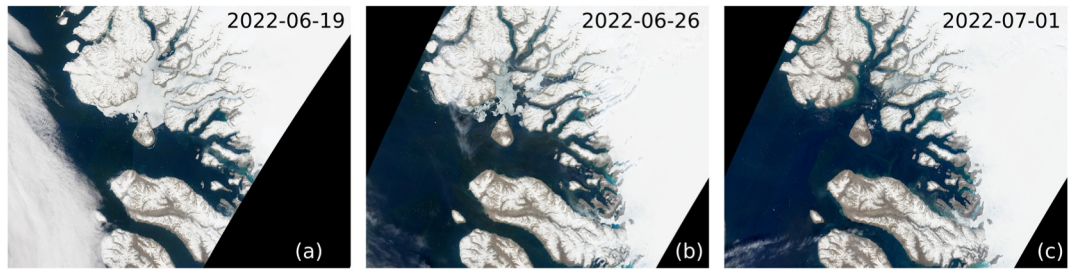


Figure 3. (a–c) Sentinel-2 images illustrating sea ice conditions obtained at the indicated days.

Atmosphérique Régional v3.11 (Delhasse et al., 2020) and 5.5 km resolution Regional Atmospheric Climate Model RACMO2.3p2 (Noël et al., 2018, 2019) data.

3. Study Site and Conditions

The Uummannaq fjord system on Greenland's northwest coast (~70–71°N, Figure 1) is a complex network of deep, glacially carved fjords opening west into Baffin Bay. The main Uummannaq Fjord extends inland over 100 km and branches into multiple tributaries (Figure 2a). Bathymetry is complex, with basins exceeding 900 m and no shallow sill at the fjord mouth. Tides are mainly semidiurnal, with a ~2 m range at Uummannaq (Danish Meteorological Institute, station 2991610), and low tidal velocities based in a barotropic 1 km resolution tide model (root mean square velocity around 0.01 m s^{-1}, and lower than 0.05 m s^{-1} throughout the fjord system Howard & Padman, 2021; Greene, Erofeeva, et al., 2024). Numerous marine and land-terminating glaciers feed the system (red lines in Figure 2a), with icebergs being present near marine-terminating glaciers. The town of Uummannaq serves as regional hub for fishing, hunting, and growing tourism, while smaller regional communities rely heavily on local marine resources.

The northern fjord branches were partly ice-covered at the start of the expedition (Sentinel-2 image from 26 June 2022, Figure 3b), but became ice-free shortly after (Figure 3c). Air temperature ranged from between 4 and 11°C, wind speeds were unusually low (<6 m s^{-1}), compared to typical wind speeds regularly exceeding 10 m s^{-1}. Most marine-terminating glaciers in the fjord system were relatively stable during the expedition, except Kangilliup Sermia (3 in Figure 2a), which retreated 200 m in late June 2022, and Salliarutsip Sermia (1 in Figure 2a), which began retreating on 9 July, totaling 400 m by 14 July (data not shown). Glacial meltwater runoff at termini started unusually late in 2022, with June values below the 1963–2023 mean (Figure 4b). July–August runoff was near the long-term average, although runoff has tended to increase since the 2000s (Figure 4a), suggesting that these values are relatively low for the current climate. Seasonal patterns were similar across termini, with roughly half the total runoff from Kangerluarsuup Sermia and half from other outlets.

The fjord's thermohaline structure features 1–7°C warm, relatively fresh (27–32 g kg^{-1}) surface water from sea ice melt and land runoff. This buoyancy input and the fjord's sheltered conditions prevent a classical surface mixed layer; the water column is strongly stratified even in the near-surface layer. Lowest surface salinities occur in northern branches with mostly land-terminating glaciers. Around 40 m, temperatures reach a minimum near or slightly below 0°C with salinity ~33 g kg^{-1}, both increasing with depth below (Figures 2a and 2b). A warm

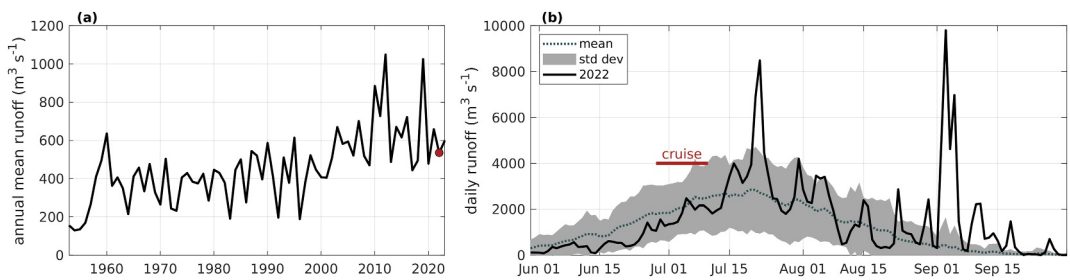


Figure 4. (a) Annual mean combined run-off from the glaciers indicated in Figure 2a, (b) daily run-off in summer 2022 (black line), 1963–2023 mean run-off (dotted line) and standard deviation (gray shading), time of the expedition indicated in red.

21699291, 2026, 11, Downloaded from https://agupubs.onlinelibrary.wiley.com/doi/10.1029/2026JC024509, Wiley Online Library on [16/11/2026]. See the Terms and Conditions (https://onlinelibrary.wiley.com/terms-and-conditions) on Wiley Online Library for rules of use; OA articles are governed by the applicable Creative Commons License

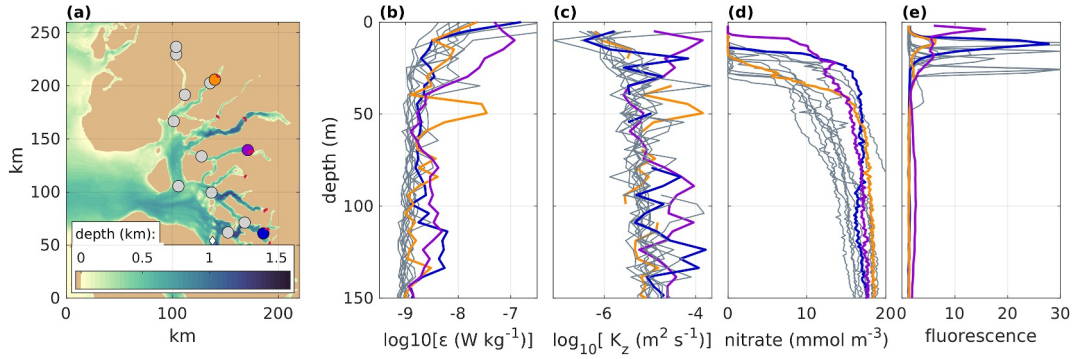


Figure 5. (a) Bathymetric map of the fjord system, with turbulence sampling positions indicated in circles and glacier termini indicated in red (see Figure 2 for the glacier names), colormap shows depth in km. Upper ocean profiles of (b) average turbulent dissipation rates ε (W kg^{-1}, logarithmic), (c) vertical diffusivity K_z (m^2 s^{-1}), (d) nitrate (mmol m^{-3}, smoothed with a 15 m moving mean for better visibility), and (e) fluorescence (uncalibrated) for each VMP and nutrient sampling station. Stations closest to glacier termini are marked in color in (a), and correspond to the bold lines in (b–e) of the same color.

subsurface core (200–400 m offshore) weakens farther into the fjord. Surface temperatures are lowest in northeastern fjords and highest in southern branches sampled later in the expedition.

4. Vertical Mixing, Nitrate Distribution and Primary Production

Turbulent kinetic energy dissipation is elevated within a 10–40 m thick surface mixing layer, but generally low (10^{-9} W kg^{-1}) at greater depths (Figure 5b). Near glacier fronts (colored lines, Figure 5b), occasional subsurface patches of elevated dissipation occur. Notably, ∼3 km from the Kangerlussuup Sermia terminus (purple, Figure 5b), turbulence is strongly enhanced in the upper 40 m, with a weaker increase below 80 m.

Vertical diffusivity (Figure 5c) ranges from 10^{-6} to 10^{-5} m^2 s^{-1} below the stratified surface layer (∼20 m) and rises to ∼10^{-5} m^2 s^{-1} below ∼120 m. Higher values (∼10^{-4} m^2 s^{-1}) occur where dissipation is elevated. These patterns agree with previous surveys in Northeast Greenland fjords (Bendtsen et al., 2021), which reported low rates below the surface layer and enhanced dissipation within 2 km of the Sermeq Kujalleq glacier front.

The fjord biogeochemistry at the time of sampling includes (near-)depleted nitrate in the surface 10–30 m (Figure 5d). The upper nitracline, that is, where nitrate begins to increase, often aligns with the depth of the local turbulent surface mixing layer. A deep chlorophyll-a maximum (based on fluorescence measurements) is consistently located near the nitracline's upper bound (Figure 5e). At the station near Kangerlussuup Sermia, where turbulence is elevated in the upper 40 m, both the nitracline and fluorescence maximum are positioned

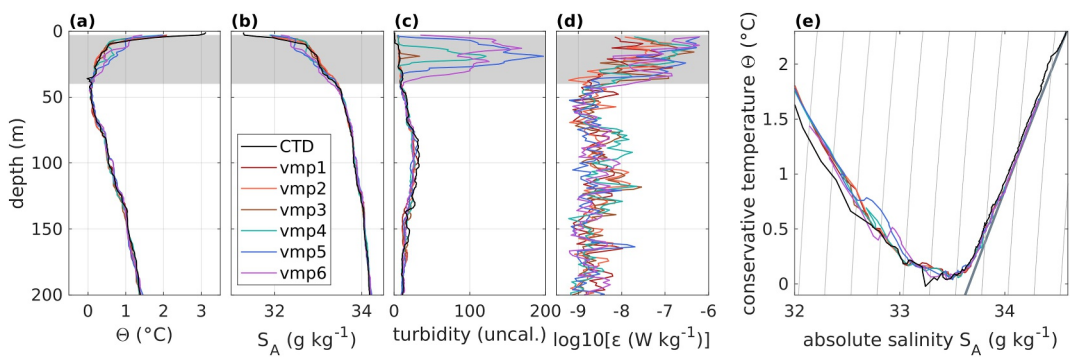


Figure 6. Vertical profiles of (a) Conservative Temperature (°C), (b) Absolute Salinity (g kg^{-1}), (c) turbidity (uncalibrated), (d) turbulent dissipation rate (W kg^{-1}), and (e) T-S diagram with isopycnals spaced at 0.2 kg m^{-3} (thin) and the Gade line (thick (Gade, 1979)), displayed in gray. Black lines refer to data from the ship-based CTD, other colors to data from the VMP operated from a workboat. Gray shading in (a–d) indicated the depth range of the detached subglacial discharge plume. All data were collected within a 300 m by 300 m area, approximately 3 km from the terminus of Kangerlussuup Sermia (station marked with purple dot in Figure 5a).

21699291, 2026, 11, Downloaded from https://agupubs.onlinelibrary.wiley.com/doi/10.1029/2026JC024509, Wiley Online Library on [16/11/2026]. See the Terms and Conditions (https://onlinelibrary.wiley.com/terms-and-conditions) on Wiley Online Library for rules of use; OA articles are governed by the applicable Creative Commons License

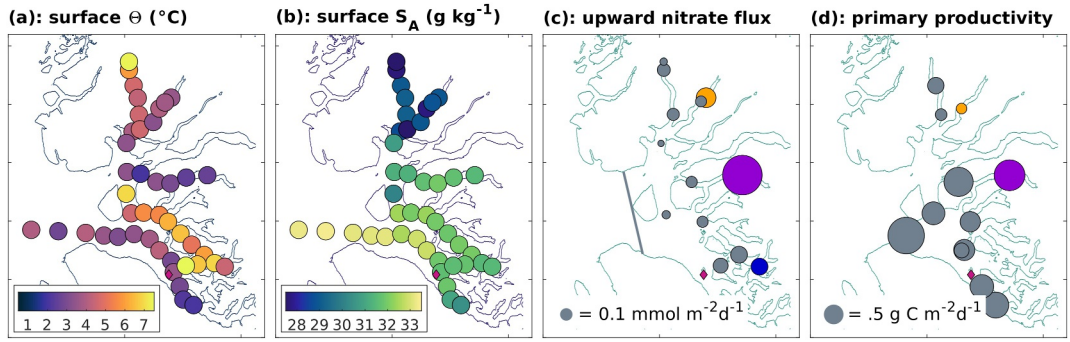


Figure 7. (a) Sea surface (0–5 m) Conservative Temperature (°C) and (b) Absolute Salinity (g kg^{-1}), (c) upward turbulent nitrate flux (mmol m^{-2} d^{-1}), and (d) primary productivity (mg C m^{-2} d^{-1}). The purple diamonds mark the location of Uummannaq, purple, orange and blue dots in (c) and (d) correspond to the glacier-adjacent stations as in Figure 5. The gray line in (c) indicates the western boundary used for integrating the fjord system total area.

shallower than at any other fjord site (purple lines, Figures 5d and 5e). In four of six VMP profiles near Kangerlussuup Sermia (Figure 6), a distinct subsurface turbidity layer occurs between 3 and 40 m, coinciding with slightly warmer, fresher water (Figures 6a and 6b) compared to ship-based CTD measurements, which did not record elevated surface turbidity (Figure 6c). We interpret this as a detached subglacial discharge plume, that is, a plume that has reached neutral buoyancy and now moves laterally away from the glacier front. Elevated dissipation rates here may be caused either by advection of convection-driven turbulence from when the plume was rising to the surface, or by turbulence generated at the interface between the faster-flowing plume and ambient fjord water. A deeper distinct turbidity layer exists at 60–140 m, with lower values and slightly elevated dissipation between 80 and 120 m, potentially from a secondary plume or sinking fine particles that are kept in suspension by turbulence in this layer.

Our sampling setup limited detailed observations of the detached plume, but Jackson et al. (2017) conducted a targeted survey in July 2014 using cross-fjord transects starting 200 m from the same glacier terminus with a remotely operated boat. They identified a subglacial discharge plume confined to the upper 40 m, consistent with our results, with peak velocities ∼0.4 m s^{-1} at 30 m. The plume was ∼1 km wide at 0.5 km from the front, expanding to ∼2 km at 15 km downstream. While clearly detectable in velocity data, it had only weak temperature and salinity signals. Temperature and salinity stratification in 2014 broadly matches our observations, though the temperature minimum near 70 m was more pronounced.

The small footprint of the detached subglacial discharge plume compared to the fjord width explains the fine-scale lateral variability in our observations, with elevated turbidity appearing only in some profiles within a 300 × 300 m region near the glacier front. A detached plume may also have been present near other glacier-front stations (orange and blue in Figure 5) but went undetected. Yet, elevated dissipation rates over the plume depth occur even in profiles without increased turbidity, suggesting that turbulence driven by the plume extends beyond the visibly turbid core.

The average vertical turbulent nitrate flux across the fjord system is 0.19 mmol m^{-2} d^{-1} (Figure 7c), peaking at 1.17 mmol m^{-2} d^{-1} near Kangerlussuup Sermia (purple in Figure 5). Excluding this outlier, the background flux averages 0.11 mmol m^{-2} d^{-1}, similar to the offshore station value of 0.10 mmol m^{-2} d^{-1} (data not shown). While the calculation of individual nutrient flux estimates is fairly robust, likely within a factor of two (Koenig et al., 2023), a greater uncertainty that cannot be quantified is associated with the statistic representativeness of the few available samples, especially associated with the intermittent nature of turbulent mixing (Baker & Gibson, 1987).

Primary production (Figure 7d) is on the order of 1000 mg C m^{-2} d^{-1}, or roughly 80 mmol C m^{-2} d^{-1}. Assuming a Redfield ratio of C:N = 106:16, this corresponds to a nitrate uptake of about 12 mmol m^{-2} d^{-1}. The variability in primary production does not exhibit any distinct spatial pattern, except for lower levels of productivity in the northern fjord branches that might be related to the very recent retreat of sea ice in that region (Figure 3).

21699291, 2026, 11, Downloaded from https://agupubs.onlinelibrary.wiley.com/doi/10.1029/2026JC024509, Wiley Online Library on [16/11/2026]. See the Terms and Conditions (https://onlinelibrary.wiley.com/terms-and-conditions) on Wiley Online Library for rules of use; OA articles are governed by the applicable Creative Commons License

21699291, 2026, 11, Downloaded from https://agupubs.onlinelibrary.wiley.com/doi/10.1029/2026JC024509, Wiley Online Library on [16/11/2026]. See the Terms and Conditions (https://onlinelibrary.wiley.com/terms-and-conditions) on Wiley Online Library for rules of use; OA articles are governed by the applicable Creative Commons License

5. Discussion

A recent synthesis of co-located Arctic turbulence and nutrient observations found vertical nutrient fluxes in Arctic waters to be roughly an order of magnitude lower than in the global ocean (Randelhoff et al., 2020). Within the Arctic, fluxes are weakest in regions with strong surface stratification caused by terrestrial freshwater input, which suppresses turbulent mixing, and strongest near complex bathymetry such as steep continental slopes, where tidal and mean flows enhance energy transfer to turbulence. The magnitude of wintertime nutrient fluxes was identified as a key control on the surface nutrient inventory at the onset of the bloom season, making regions of winter deep convection potential hotspots of productivity (Randelhoff et al., 2020).

Nitrate fluxes of about 0.1 mmol m^{-2} d^{-1} reported here, away from the subglacial discharge plumes, fall well within the typical Arctic range (Randelhoff et al., 2020, their Figure 8). Fluxes in the central Arctic Ocean and the Siberian shelf seas are about an order of magnitude smaller (Randelhoff et al., 2020), whereas episodic strong mixing events above the continental slope, driven by atmospheric forcing, can reach up to 0.3 mmol m^{-2} d^{-1} and may contribute disproportionately to regional nutrient transport (Schulz et al., 2022). In contrast, fluxes in the Barents Sea, Fram Strait, and around Yermak Plateau can be comparable to or up to an order of magnitude higher than those observed in the Uummannaq fjord system in early summer. The only available nitrate flux data from a Greenland fjord are from Young Sound in northeast Greenland, a fjord system without marine-terminating glaciers. There, average summer nitrate fluxes of 0.035 mmol m^{-2} d^{-1} are about 20% of those measured near Uummannaq, while elevated values of 0.33 mmol m^{-2} d^{-1}, roughly a third of the flux near the detached subglacial plume, occur near the Young Sound sill, likely due to enhanced mixing over steep topography (Boone et al., 2017; Randelhoff et al., 2020).

Despite glaciated fjords hosting highly productive ecosystems, the observed turbulent nutrient fluxes here are relatively low compared to global values and are close to the Arctic average (Randelhoff et al., 2020). This contrast points to the importance of transport processes beyond turbulent mixing that make substantial contributions to the surface nutrient budget. In the following, we attempt to assess the fjord-scale vertical nitrate supply by different processes and nitrate consumption by primary production, keeping in mind that the limited available measurements may not be statistically representative and that our estimates can therefore only provide an order-of-magnitude assessment. We define the sea-ward bound of the fjord area as the gray line in Figure 7c just west of the island Illorsuit, resulting in a fjord area of 8,500 km^2. This boundary is somewhat arbitrary, but the resulting estimates scale linearly with the area considered.

- *Background vertical mixing in the fjord*: An average vertical nutrient flux of 0.11 mmol m^{-2} d^{-1} (excluding the high value in the detached plume) over the total Uummannaq fjord system area of 8,500 km^2 gives a background transport of 9.4×10^8 mmol d^{-1}.
- *Detached subglacial discharge plume*: Integrating the turbulent nitrate flux near the detached plume of 1.17 mmol m^{-2} d^{-1} over a 1 km plume width (Jackson et al., 2017) and assuming a 5 km downstream distance of elevated turbulence yields a total vertical nitrate supply of about 6×10^6 mmol d^{-1}.
- *Rising subglacial discharge plume*: From the presented observations, we cannot quantify the initial contribution of the rising portion of the plume, when subglacial discharge exits at depth, entrains ambient deep water, and thereby transports nutrient-rich water upward as it ascends. We hence draw on data from Jackson et al. (2017). Their analysis suggests that entrainment into the plume after detachment from the glacier front is minimal, meaning that once the buoyant discharge separates from the terminus, little additional fjord water is mixed in as the plume travels horizontally away from the glacier. It should be noted, however, that entrainment within the first 500 m of the terminus is not well constrained by their data. The plume itself is estimated to contain only 4.4% freshwater, implying that the remaining 95.6% is entrained ambient water (Jackson et al., 2017). Assuming negligible entrainment after detachment, a total plume volume flux of 6,600 ± 1,300 m^3 s^{-1} (Jackson et al., 2017), and a deep-water nitrate concentration of 16 mmol m^{-3} (our data, Figure 5d), the resulting upward nitrate transport in the rising plume is approximately 9×10^9 mmol d^{-1}.
- *System-wide supply by discharge plumes*: Nutrient fluxes will vary among individual plumes and over time, however, their common characteristics allow us to estimate their transport potential from the nutrient concentrations in deeper waters and the subglacial discharge volume flux. Generally, strong entrainment is found to rapidly dilute the original glacier-derived water as the plume rises, such that the fraction of glacier water is small by the time the plume reaches its terminal depth. A pan-Greenland modeling study estimates glacier-

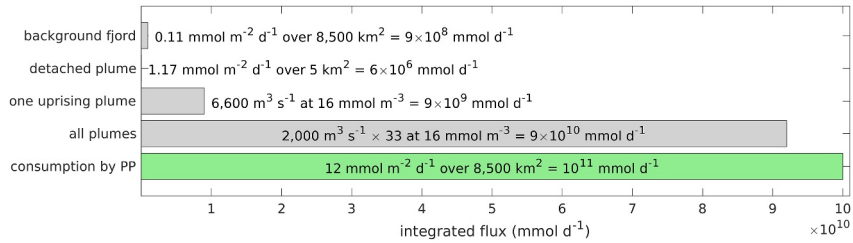


Figure 8. Estimated surface nitrate supply (gray) and consumption by primary production (green) for the Uummannaq fjord system.

water fractions of only 1.3%–3.3% when plumes reach their neutral density or the surface (Slater et al., 2022), observations from Sermilik Fjord find a fraction of approximately 3% glacier water, with 88% of the exported plume water consisting of nutrient-rich Atlantic Water (Beaird et al., 2018). For sufficiently deep glacier termini, where plumes rise through nutrient-rich subsurface waters over most of their ascent, the nutrient concentrations of the final plume can therefore be expected to approach those of the ambient deep water. Assuming a total subglacial discharge in the system of 2,000 $m^3\ s^{-1}$ during the time of sampling (Figure 4b) making up 3% of the final plume volume with a nitrate concentration of 16 mmol m^{-3} as above yields a total upward transport of 9.2×10^{10} mmol d^{-1} associated with subglacial discharge.

Comparing these nutrient supply mechanisms (Figure 8), we find that nutrient supply from elevated mixing near the detached plume is negligible on a fjord-scale, but might still be of local significance, as elevated turbidity within the plume and the distinct biogeochemical signature of plume waters may create important small-scale ecological gradients near glacier fronts. Nutrient transport by a single subglacial plume can exceed the nutrient supply by background mixing by an order of magnitude. Cumulative transport via rising subglacial discharge in the fjord system is likely greater by one order of magnitude. According to buoyant plume theory, plume volume flux scales with $Q_{sg}^{\frac{1}{3}}$, where Q_{sg} is subglacial discharge (e.g., Hewitt, 2020; Straneo & Cenedese, 2015). Increasing discharge is hence expected to enhance nutrient fluxes until the mechanism ceases when glacier fronts become too shallow or retreat onto land.

In addition to the mechanisms discussed above, several other processes may influence turbulence and nutrient transport in the fjord. Ice melange can modify how wind generates near-surface turbulence, while freshwater input from melting strengthens surface stratification and may suppress mixing. Grounded icebergs create obstacles that can generate turbulence from the mean flow, and rising meltwater can entrain deep, nutrient-rich water. Calving events (Inall et al., 2026) and interactions with steep fjord walls, sills, and other bathymetric features may also enhance vertical mixing. Tidal forcing is negligible in this system, with root-mean-square tidal velocities around 0.01 m s^{-1} (Greene, Erofeeva, et al., 2024; Howard & Padman, 2021), though tides are likely important in fjords with stronger tidal currents (Mortensen et al., 2022). As the melt season progresses, increasing subglacial discharge and extreme events, such as sudden drainage of supraglacial lakes (Kjeldsen et al., 2014; Schiøtt et al., 2022), can drive more vigorous mixing. However, increased buoyancy input in the surface layer by iceberg melt and terrestrial runoff can increase upper ocean stratification and hence suppress vertical mixing and nitrate fluxes (Holding et al., 2019).

Observed primary production during the time of sampling is on the order of 1000 mg C $m^{-2}\ d^{-1}$, corresponding to a nitrate uptake of 12 mmol $m^{-2}\ d^{-1}$. Surface nitrate concentrations are depleted in the upper 10–20 m (Figure 5d), and the system is transitioning toward a subsurface bloom with the Chlorophyll-a maximum situated at 10–30 m depth (Figure 5e). Primary production will therefore depend increasingly on the supply of new nutrients to the euphotic zone. The turbulent nitrate fluxes measured here can sustain only about 1% of the observed primary production. However, when adding the estimated nutrient transport associated with subglacial discharge plumes, the combined nitrate supply has the potential to support primary production at levels comparable to those observed here (Figure 8). All these estimates rely on few measurements, neglect horizontal advection of nutrients out of the fjord system, and assume that rising subglacial discharge plumes deliver deep nutrients all the way to the euphotic zone, which is the case for the observed plume (Figure 6), but other plumes might reside subsurface. Further work is needed to robustly quantify the relative contributions and seasonal evolution of the different transport processes that regulate surface nutrient availability and primary production in fjord systems.

21699291, 2026, 11, Downloaded from https://agupubs.onlinelibrary.wiley.com/doi/10.1029/2026JC024509, Wiley Online Library on [16/11/2026]. See the Terms and Conditions (https://onlinelibrary.wiley.com/terms-and-conditions) on Wiley Online Library for rules of use; OA articles are governed by the applicable Creative Commons License

21699291, 2026, 11, Downloaded from https://agupubs.onlinelibrary.wiley.com/doi/10.1029/2026JC024509, Wiley Online Library on [16/11/2026]. See the Terms and Conditions (https://onlinelibrary.wiley.com/terms-and-conditions) on Wiley Online Library for rules of use; OA articles are governed by the applicable Creative Commons License

6. Conclusions

During early summer, turbulent vertical nutrient fluxes in the Uummannaq fjord system, away from the subglacial discharge plumes, are around 0.1 mmol m^{-2} d^{-1}. Integrated over the fjord, this flux is an order of magnitude smaller than the estimated nutrient supply from a single rising subglacial discharge plume. Beyond this initial entrainment-driven transport, our observations reveal a secondary mechanism: sustained turbulence in the detached plume downstream of the glacier front. Although less efficient than upward transport during plume ascent, this process may be locally important. At this time of year, primary production is not nutrient-limited, but this balance is expected to change as the bloom progresses.

In fjords without marine-terminating glaciers and subglacial discharge plumes, nutrient supply to the surface ocean in spring and summer would be greatly reduced, likely affecting ecosystem productivity and the communities that depend on it ecologically, economically, and culturally. Identifying alternative nutrient supply mechanisms and potential productivity hotspots is essential to assess which fjords may remain productive in a future without marine-terminating glaciers. Additionally, trends in sea ice cover and suspended sediments, which influence light availability, must be considered alongside nutrient supply when interpreting spatial and temporal patterns of primary production in Greenland's fjords.

Conflict of Interest

The authors declare no conflicts of interest relevant to this study.

Availability Statement

Data used in this publication is available via Schulz (2025) for the vertical microstructure profiler (VMP250) data, Ollevier et al. (2023) for the ship-based CTD data, and Meire (2026) for the nitrate and primary production data.

Acknowledgments

KS, LM and SM received funding through the US National Science Foundation Grant NSF-OPP 2335928. KXZ received funding through US National Foundation Grants NSF-OCE 2319494 and NSF-OPP 2138790. DF acknowledges support from Novo Nordisk foundation Grant NNF23OC00807040. Ship time onboard R/V Sanna was provided to the "Innovative study on regional high resolution imaging of glacier induced plankton dynamics in West-Greenland fjords (IOPD)" campaign (seadatanet.org: ID 21026654) by the Eurofleets+ project which received funding from the European Union H2020 Research and Innovation Program under Grant agreement 824077. The turbulence profiler used for this study was made available by Arctic Research Centre - Aarhus University. We are thankful to the participants, engineers and the crew onboard the R/V Sanna for their support during the cruise, and for the helpful reviews provided by Ken Hughes and an anonymous reviewer.

References

Ardyna, M., & Arrigo, K. R. (2020). Phytoplankton dynamics in a changing Arctic Ocean. *Nature Climate Change*, *10*(10), 892–903. https://doi.org/10.1038/s41558-020-0905-y

Baker, M. A., & Gibson, C. H. (1987). Sampling turbulence in the stratified ocean: Statistical consequences of strong intermittency. *Journal of Physical Oceanography*, *17*(10), 1817–1836. https://doi.org/10.1175/1520-0485(1987)017⟨1817:STITSO⟩2.0.CO;2

Beaird, N. L., Straneo, F., & Jenkins, W. (2018). Export of strongly diluted Greenland meltwater from a major glacial fjord. *Geophysical Research Letters*, *45*(9), 4163–4170. https://doi.org/10.1029/2018GL077000

Bendtsen, J., Rysgaard, S., Carlson, D. F., Meire, L., & Sejr, M. K. (2021). Vertical mixing in stratified fjords near tidewater outlet glaciers along Northwest Greenland. *Journal of Geophysical Research: Oceans*, *126*(8), e2020JC016898. https://doi.org/10.1029/2020JC016898

Boone, W., Rysgaard, S., Kirillov, S., Dmitrenko, I., Bendtsen, J., Mortensen, J., et al. (2017). Circulation and fjord-shelf exchange during the ice-covered period in Young Sound-Tyrolerfjord, Northeast Greenland (74 N). Estuarine. *Coastal and Shelf Science*, *194*, 205–216. https://doi.org/10.1016/j.ecss.2017.06.021

Bouffard, D., & Boegman, L. (2013). A diapycnal diffusivity model for stratified environmental flows. *Dynamics of Atmospheres and Oceans*, *61*, 14–34. https://doi.org/10.1016/j.dynatmoce.2013.02.002

Cape, M. R., Straneo, F., Beaird, N., Bundy, R. M., & Charette, M. A. (2019). Nutrient release to oceans from buoyancy-driven upwelling at Greenland tidewater glaciers. *Nature Geoscience*, *12*(1), 34–39. https://doi.org/10.1038/s41561-018-0268-4

Catania, G., Stearns, L. A., Sutherland, D. A., Fried, M. J., Bartholomaus, T. C., Morlighem, M., et al. (2018). Geometric controls on tidewater glacier retreat in central western Greenland. *Journal of Geophysical Research: Earth Surface*, *123*(8), 2024–2038. https://doi.org/10.1029/2017JF004499

Delhasse, A., Kittel, C., Amory, C., Hofer, S., Van As, D., S. Fausto, R., & Fettweis, X. (2020). Brief communication: Evaluation of the near-surface climate in ERA5 over the Greenland Ice Sheet. *The Cryosphere*, *14*(3), 957–965. https://doi.org/10.5194/tc-14-957-2020

Fahrner, D., Lea, J. M., Brough, S., Mair, D. W., & Abermann, J. (2021). Linear response of the Greenland ice sheet's tidewater glacier terminus positions to climate. *Journal of Glaciology*, *67*(262), 193–203. https://doi.org/10.1017/jog.2021.13

Gade, H. G. (1979). Melting of ice in sea water: A primitive model with application to the Antarctic ice shelf and icebergs. *Journal of Physical Oceanography*, *9*(1), 189–198. https://doi.org/10.1175/1520-0485(1979)009<0189:moiisw>2.0.co;2

Goliber, S., Black, T., Catania, G., Lea, J. M., Olsen, H., Cheng, D., et al. (2022). TermPicks: A century of Greenland glacier terminus data for use in machine learning applications. *The Cryosphere*, *16*(8), 3215–3233. https://doi.org/10.5194/tc-16-3215-2022

Greene, C. A., Erofeeva, S., Padman, L., Howard, S. L., Sutterley, T., & Egbert, G. (2024). Tide model driver for matlab. *Journal of Open Source Software*, *9*(95), 6018. https://doi.org/10.21105/joss.06018

Greene, C. A., Gardner, A. S., Wood, M., & Cuzzone, J. K. (2024). Ubiquitous acceleration in Greenland Ice Sheet calving from 1985 to 2022. *Nature*, *625*(7995), 523–528. https://doi.org/10.1038/s41586-023-06863-2

Hewitt, I. J. (2020). Subglacial plumes. *Annual Review of Fluid Mechanics*, *52*(1), 145–169. https://doi.org/10.1146/annurev-fluid-010719-060252

Holding, J. M., Markager, S., Juul-Pedersen, T., Paulsen, M. L., Møller, E. F., Meire, L., & Sejr, M. K. (2019). Seasonal and spatial patterns of primary production in a high-latitude fjord affected by Greenland Ice Sheet run-off. *Biogeosciences*, *16*(19), 3777–3792. https://doi.org/10.5194/bg-16-3777-2019

Hopwood, M. J., Carroll, D., Browning, T., Meire, L., Mortensen, J., Krisch, S., & Achterberg, E. P. (2018). Non-linear response of summertime marine productivity to increased meltwater discharge around Greenland. *Nature Communications*, *9*(1), 3256. https://doi.org/10.1038/s41467-018-05488-8

Hopwood, M. J., Carroll, D., Dunse, T., Hodson, A., Holding, J. M., Iriarte, J. L., et al. (2020). How does glacier discharge affect marine biogeochemistry and primary production in the Arctic? *The Cryosphere*, *14*(4), 1347–1383. https://doi.org/10.5194/tc-14-1347-2020

Howard, S., & Padman, L. (2021). *Gr1kmtm: Greeland 1 kilometer tide model*. Arctic data center. https://doi.org/10.18739/A2B853K18

Inall, M., Fraser, N., Sundfjord, A., & Meredith, M. P. (2026). Glacial ice-front calving: Internal wave generation and melting. *Geophysical Research Letters*, *53*(11), e2026GL122121. https://doi.org/10.1029/2026GL122121

Jackson, R. H., Shroyer, E. L., Nash, J. D., Sutherland, D. A., Carroll, D., Fried, M. J., et al. (2017). Near-glacier surveying of a subglacial discharge plume: Implications for plume parameterizations. *Geophysical Research Letters*, *44*(13), 6886–6894. https://doi.org/10.1002/2017GL073602

Kanna, N., Sugiyama, S., Ando, T., Wang, Y., Sakuragi, Y., Hazumi, T., et al. (2022). Meltwater discharge from marine-terminating glaciers drives biogeochemical conditions in a Greenlandic fjord. *Global Biogeochemical Cycles*, *36*(11), e2022GB007411. https://doi.org/10.1029/2022GB007411

Kanna, N., Sugiyama, S., Fukamachi, Y., Nomura, D., & Nishioka, J. (2020). Iron supply by subglacial discharge into a fjord near the front of a marine-terminating glacier in northwestern Greenland. *Global Biogeochemical Cycles*, *34*(10), e2020GB006567. https://doi.org/10.1029/2020GB006567

Kanna, N., Sugiyama, S., Ohashi, Y., Sakakibara, D., Fukamachi, Y., & Nomura, D. (2018). Upwelling of macronutrients and dissolved inorganic carbon by a subglacial freshwater driven plume in Bowdoin Fjord, northwestern Greenland. *Journal of Geophysical Research: Biogeosciences*, *123*(5), 1666–1682. https://doi.org/10.1029/2017JG004248

Kjeldsen, K. K., Mortensen, J., Bendtsen, J., Petersen, D., Lennert, K., & Rysgaard, S. (2014). Ice-dammed lake drainage cools and raises surface salinities in a tidewater outlet glacier fjord, West Greenland. *Journal of Geophysical Research: Earth Surface*, *119*(6), 1310–1321. https://doi.org/10.1002/2013JF003034

Kochtitzky, W., & Copland, L. (2022). Retreat of Northern Hemisphere marine-terminating glaciers, 2000–2020. *Geophysical Research Letters*, *49*(3), e2021GL096501. https://doi.org/10.1029/2021GL096501

Koenig, Z., Fer, I., Chierici, M., Fransson, A., Jones, E., & Kolås, E. H. (2023). Diffusive and advective cross-frontal fluxes of inorganic nutrients and dissolved inorganic carbon in the Barents Sea in autumn. *Progress in Oceanography*, *219*, 103161. https://doi.org/10.1016/j.pocean.2023.103161

Lea, J. M. (2018). The Google Earth Engine Digitisation Tool (GEEDiT) and the Margin change Quantification Tool (MaQiT)–simple tools for the rapid mapping and quantification of changing Earth surface margins. *Earth Surface Dynamics*, *6*(3), 551–561. https://doi.org/10.5194/esurf-6-551-2018

Lee, S. H., Joo, H. M., Liu, Z., Chen, J., & He, J. (2012). Phytoplankton productivity in newly opened waters of the Western Arctic Ocean. *Deep Sea Research Part II: Topical Studies in Oceanography*, *81*, 18–27. https://doi.org/10.1016/j.dsr2.2011.06.005

Lueck, R., Fer, I., Bluteau, C., Dengler, M., Holtermann, P., Inoue, R., et al. (2024). Best practices recommendations for estimating dissipation rates from shear probes. *Frontiers in Marine Science*, *11*, 1334327. https://doi.org/10.3389/fmars.2024.1334327

Mankoff, K. D. (2020). Streams, Outlets, Basins, and Discharge [k=1.0]. *GEUS Dataverse*. https://doi.org/10.22008/FK2/XKQVL7

Mankoff, K. D., Noël, B., Fettweis, X., Ahlstrøm, A. P., Colgan, W., Kondo, K., et al. (2020). Greenland liquid water discharge from 1958 through 2019. *Earth System Science Data*, *12*(4), 2811–2841. https://doi.org/10.5194/essd-12-2811-2020

McDougall, T. J., & Barker, P. M. (2011). *Getting started with TEOS-10 and the Gibbs Seawater (GSW) Oceanographic Toolbox*. SCOR/IAPSO. Retrieved from www.TEOS-10.org

Meire, L. (2026). Nitrate and primary production dataset from the fjords around Uummannaq, Northwest Greenland [Dataset]. *Zenodo*. https://doi.org/10.5281/zenodo.18338891

Meire, L., Mortensen, J., Meire, P., Juul-Pedersen, T., Sejr, M. K., Rysgaard, S., et al. (2017). Marine-terminating glaciers sustain high productivity in Greenland fjords. *Global Change Biology*, *23*(12), 5344–5357. https://doi.org/10.1111/gcb.13801

Meire, L., Paulsen, M. L., Meire, P., Rysgaard, S., Hopwood, M. J., Sejr, M. K., et al. (2023). Glacier retreat alters downstream fjord ecosystem structure and function in Greenland. *Nature Geoscience*, *16*(8), 671–674. https://doi.org/10.1038/s41561-023-01218-y

Meire, L., Søgaard, D., Mortensen, J., Meysman, F., Soetaert, K., Arendt, K., et al. (2015). Glacial meltwater and primary production are drivers of strong CO_2 uptake in fjord and coastal waters adjacent to the Greenland Ice Sheet. *Biogeosciences*, *12*(8), 2347–2363. https://doi.org/10.5194/bg-12-2347-2015

Morlighem, M., Williams, C., Rignot, E., An, L., Arndt, J. E., Bamber, J., et al. (2022). Icebridge bedmachine Greenland, version 5 [Dataset]. *NASA National Snow and Ice Data Center Distributed Active Archive Center*. https://doi.org/10.5067/GMEVBWFLWA7X

Mortensen, J., Rysgaard, S., Winding, M., Juul-Pedersen, T., Arendt, K., Lund, H., et al. (2022). Multidecadal water mass dynamics on the West Greenland Shelf. *Journal of Geophysical Research: Oceans*, *127*(7), e2022JC018724. https://doi.org/10.1029/2022JC018724

Noël, B., Van De Berg, W. J., Lhermitte, S., & Van Den Broeke, M. R. (2019). Rapid ablation zone expansion amplifies north Greenland mass loss. *Science Advances*, *5*(9), eaaw0123. https://doi.org/10.1126/sciadv.aaw0123

Noël, B., Van De Berg, W. J., Van Wessem, J. M., Van Meijgaard, E., Van As, D., Lenaerts, J., et al. (2018). Modelling the climate and surface mass balance of polar ice sheets using RACMO2–Part 1: Greenland (1958–2016). *The Cryosphere*, *12*(3), 811–831. https://doi.org/10.5194/tc-12-811-2018

Ollevier, A., Meire, L., Bladfort, D., Develter, R., Möller, K. O., Planken, K., et al. (2023). Data from IOPD cruise Part 1 Physical and imaging data [Dataset]. *Marine Data Archive*. Retrieved from https://marineinfo.org/doc/dataset/8430

Osborn, T. (1980). Estimates of the local rate of vertical diffusion from dissipation measurements. *Journal of Physical Oceanography*, *10*(1), 83–89. https://doi.org/10.1175/1520-0485(1980)010⟨0083:EOTLRO⟩2.0.CO;2

Plant, J. N., Sakamoto, C. M., Johnson, K. S., Maurer, T. L., & Bif, M. B. (2023). Updated temperature correction for computing seawater nitrate with in situ ultraviolet spectrophotometer and submersible ultraviolet nitrate analyzer nitrate sensors. *Limnology and Oceanography: Methods*, *21*(10), 581–593. https://doi.org/10.1002/lom3.10566

Randelhoff, A., Fer, I., Sundfjord, A., Tremblay, J.-É., & Reigstad, M. (2016). Vertical fluxes of nitrate in the seasonal nitracline of the Atlantic sector of the Arctic Ocean. *Journal of Geophysical Research: Oceans*, *121*(7), 5282–5295. https://doi.org/10.1002/2016JC011779

Randelhoff, A., Holding, J., Janout, M., Sejr, M. K., Babin, M., Tremblay, J.-É., & Alkire, M. B. (2020). Pan-Arctic Ocean primary production constrained by turbulent nitrate fluxes. *Frontiers in Marine Science*, *7*, 150. https://doi.org/10.3389/fmars.2020.00150

Rudels, B., Larsson, A.-M., & Sehlstedt, P.-I. (1991). Stratification and water mass formation in the Arctic Ocean: Some implications for the nutrient distribution. *Polar Research*, *10*(1), 19–32. https://doi.org/10.1111/j.1751-8369.1991.tb00631.x

21699291, 2026, 11, Downloaded from https://agupubs.onlinelibrary.wiley.com/doi/10.1029/2026JC024509, Wiley Online Library on [16/11/2026]. See the Terms and Conditions (https://onlinelibrary.wiley.com/terms-and-conditions) on Wiley Online Library for rules of use; OA articles are governed by the applicable Creative Commons License

Sakamoto, C. M., Johnson, K. S., & Coletti, L. J. (2009). Improved algorithm for the computation of nitrate concentrations in seawater using an in situ ultraviolet spectrophotometer. *Limnology and Oceanography: Methods*, *7*(1), 132–143. https://doi.org/10.4319/lom.2009.7.132

Sakamoto, C. M., Johnson, K. S., Coletti, L. J., & Jannasch, H. W. (2017). Pressure correction for the computation of nitrate concentrations in seawater using an in situ ultraviolet spectrophotometer. *Limnology and Oceanography: Methods*, *15*(10), 897–902. https://doi.org/10.1002/lom3.10209

Schiøtt, S., Tejsner, P., & Rysgaard, S. (2022). Inuit and local knowledge on the marine ecosystem in Ilulissat Icefjord, Greenland. *Human Ecology*, *50*(1), 167–181. https://doi.org/10.1007/s10745-021-00277-2

Schulz, K. (2025). Ocean turbulent dissipation rates in the fjords around Uummannaq, Northwest Greenland, derived from a vertical microstructure profiler equipped with shear probes in summer 2022 [Dataset]. *Arctic Data Center*. https://doi.org/10.18739/A28W3844S

Schulz, K., Lincoln, B., Povazhnyy, V., Rippeth, T., Lenn, Y.-D., Janout, M., et al. (2022). Increasing nutrient fluxes and mixing regime changes in the eastern Arctic Ocean. *Geophysical Research Letters*, *49*(5), e2021GL096152. https://doi.org/10.1029/2021GL096152

Slater, D., Carroll, D., Oliver, H., Hopwood, M., Straneo, F., Wood, M., et al. (2022). Characteristic depths, fluxes, and timescales for Greenland's tidewater glacier fjords from subglacial discharge-driven upwelling during summer. *Geophysical Research Letters*, *49*(10), e2021GL097081. https://doi.org/10.1029/2021GL097081

Straneo, F., & Cenedese, C. (2015). The dynamics of Greenland's glacial fjords and their role in climate. *Annual Review of Marine Science*, *7*(1), 89–112. https://doi.org/10.1146/annurev-marine-010213-135133

Stuart-Lee, A. E., Mortensen, J., Juul-Pedersen, T., Middelburg, J., Soetaert, K., Hopwood, M. J., et al. (2023). Influence of glacier type on bloom phenology in two Southwest Greenland fjords. *Estuarine, Coastal and Shelf Science*, *284*, 108271. https://doi.org/10.1016/j.ecss.2023.108271

Waite, A. M., Lane, A., Carmack, E., Danielson, S. L., Ellingsen, I., Fer, I., et al. (2026). A quantitative comparison of the physical supply and biological uptake of new nitrogen in the Arctic Ocean. *Nature Reviews Earth & Environment*, *7*(5), 1–18. https://doi.org/10.1038/s43017-026-00769-z

Zheng, B., Crockford, E. T., Zhang, W., Ji, R., & Sosik, H. M. (2024). Bias-corrected high-resolution vertical nitrate profiles from the CTD rosette-mounted submersible ultraviolet nitrate analyzer. *Limnology and Oceanography: Methods*, *22*(12), 889–902. https://doi.org/10.1002/lom3.10656

21699291, 2026, 11, Downloaded from https://agupubs.onlinelibrary.wiley.com/doi/10.1029/2026JC024509, Wiley Online Library on [16/11/2026]. See the Terms and Conditions (https://onlinelibrary.wiley.com/terms-and-conditions) on Wiley Online Library for rules of use; OA articles are governed by the applicable Creative Commons License